Hindawi
Shock and Vibration
Volume 2020, Article ID 8880789, 16 pages
https://doi.org/10.1155/2020/8880789

Research Article

Influence of Inlet Angle of Guide Vane on Hydraulic Performance of an Axial Flow Pump Based on CFD

Lei Xu,[1] **Dongtao Ji**,[1] **Wei Shi**,[2] **Bo Xu**,[1] **Weigang Lu**,[1] **and Linguang Lu**[1]

[1]*College of Hydraulic Science and Engineering, Yangzhou University, Yangzhou 225009, China*
[2]*Jiangsu Water Supply Co., Ltd. In Eastern Route of S-to-N Water Diversion Project, Nanjing 210029, China*

Correspondence should be addressed to Lei Xu; leixu@yzu.edu.cn

Received 24 September 2020; Revised 24 November 2020; Accepted 5 December 2020; Published 19 December 2020

Academic Editor: Yong Zhu

Axial flow pump has been widely used in hydraulic engineering, agriculture engineering, water supply and sewerage works, and shipbuilding industry. In order to improve the hydraulic performance of pump under off-design working conditions, the influence of the inlet segment axial chord and inlet angle adjustment of the guide vane on the pump segment efficiency and flow filed was simulated by using the renormalization group (RNG) $k-\varepsilon$ turbulent model based on the Reynolds-averaged Navier–Stokes equations. The results indicate that the inlet segment axial chord and inlet angle adjustment of guide vane have a strong influence on the pump segment efficiency. Considering the support function and hydraulic loss of the guide vane, the inlet segment axial chord is set to 0.25 times the axial chord of guide vane. On the basis of the inlet angle of the guide vane under design conditions, when the inlet segment angle is turned counterclockwise, the pump segment efficiency is improved in the lower flow rate region; moreover, the pump segment efficiency is improved in the larger flow rate region when the inlet segment angle is turned clockwise. As the conditions deviate from the design working conditions, the influence of the guide vane inlet angle on the pump segment efficiency increases. If the inlet segment angle is properly adjusted under off-design working conditions, the flow pattern in the guide vane is improved and the hydraulic loss is decreased, because the inlet segment angle matches with the flow direction of impeller outlet; consequently, the pump segment efficiency is increased.

1. Introduction

Vane pump is widely used in mechanical engineering, hydraulic engineering, civil engineering, and military industry. The application of vane pump is affected by its stable and efficient operation. Therefore, it is necessary to pay attention to the optimization of the pump [1–4], and paying attention to the research on pressure pulsation, cavitations, vibration, and noise is also necessary [5–8]. Axial flow pump is a kind of vane pump with high specific speed, which is characterized by low head and large discharge rate. Due to the characteristics, axial flow pump is widely applied to low head pumping stations in the fields of water resource allocation, water environment improvement, urban flood control, irrigation, and drainage. The guide vane is an important part of the axial flow pump that is used to recover the kinetic energy of the flow at the impeller outlet [9, 10]. The hydraulic performance of guide vane has great influence on the hydraulic performance of axial flow pump and pump system. Therefore, it is of great significance to study the matching of guide vane and impeller to improve the hydraulic performance of axial flow pump.

At present, studies on the effect of the guide vane on the hydraulic performance of an axial flow pump can be summarized as follows. Li et al. [11] studied the ability of the guide vane to recover rotational kinetic energy, and Hu et al. [12] and Durmus Kaya [13] studied the influence of the guide vane on the pump efficiency for cases with and without a guide vane. Zhou et al. [14] studied the pump efficiency for different guide vanes, and Shi et al. [15] studied the hydraulic characteristics of axial flow pumps with different guide vane sweep angles. Liu et al. [16] studied the hydraulic characteristics of an axial flow pump with different numbers of guide vane panels, and Luo et al. [17] and Feng et al. [18]

studied the influence of the guide vane on the hydraulic performance of the pump system.

The guide vane is used to undertake the flow from the impeller outlet and recycle tangential energy. For the design working conditions, the guide vane inlet angle matches the flow direction of the impeller outlet. For off-design working conditions, the inlet angle of the guide vane is inconsistent with the flow direction of the impeller outlet, which leads to an increased hydraulic loss of the guide vane and a reduced axial flow pump efficiency. In recent years, some studies have explored adjusting the guide vane angle and its effect on the hydraulic performance of an axial flow pump under off-design working conditions; the results indicate that a complete adjustment of the guide vane angle improves the flow pattern in the guide vane and reduces the hydraulic loss, with a head improvement of 0.4964 m and a pump efficiency improvement of 2.1648% measured in [19]. Yang et al. [20, 21] studied a complete adjustment of the guide vane angle and its effect on the hydraulic performance of an axial flow pump system; the results indicate that the high efficiency area moves to a large discharge rate when the angle is rotated clockwise and to a small discharge rate when the angle is rotated counterclockwise. Qian et al. [22] found that when the whole angle of the guide vane is adjusted in the saddle zone, the head increases by 0.15 m, the efficiency increases by 1.93%, and the flow pattern in the axial flow pump is substantially improved. The abovementioned studies are all about the whole guide vane rotates. Thus far, no studies on matching the inlet angle of the guide vane with the flow direction of the impeller outlet for an axial flow pump have been reported.

On the one hand, the guide vane of an axial flow pump takes the flow from the impeller outlet; on the other hand, the guide vane needs to support the guide-bearing seat [23]. To avoid affecting the support function of the guide vane, in this work, the guide vane is divided into inlet segment, middle segment, and outlet segment. The inlet segment angle is adjustable, while the middle and outlet segments are fixed and used to support the guide-bearing seat. CFD method has been widely used in the studies of pump [24–31] and other aspect [32–38]. In this paper, based on the TJ04-ZL-06 pump model, which has 3 impeller blade components and 5 guide vane components [39], influence of inlet angle of guide vane on hydraulic performance was studied using a 3D turbulent flow numerical simulation. According to the numerical simulation results, the reason of the influence of inlet angle of guide vane on the hydraulic performance was analyzed. The study work has important reference value for the hydraulic design and hydraulic performance improvement of an axial flow pump.

2. Mathematical Model and Numerical Setting

2.1. Governing Equations and Turbulent Model. A 3D turbulent flow numerical simulation for an axial flow pump is established by solving the Reynolds-averaged Navier–Stokes equations [40, 41] using FLUENT software.

The fluid flow in the axial flow pump is considered incompressible. The method of steady flow numerical simulation is used to study the flow and hydraulic performance of the pump. The governing equations that are applied to solve the flow field in the pump include a continuity equation, momentum equations, and k equation and ε equation of the $k-\varepsilon$ turbulent model. The Reynolds-averaged Navier–Stokes equations are shown as follows:

$$\frac{\partial \rho}{\partial t} + \rho \frac{\partial \overline{u_i}}{\partial x_i} = 0,$$

$$\rho \frac{\partial \overline{u_i}}{\partial t} + \rho \frac{\partial \overline{u_i u_j}}{\partial x_j} = -\frac{\partial \overline{p}}{\partial x_i} + \frac{\partial}{\partial x_j}\left[\mu\left(\frac{\partial \overline{u_i}}{\partial x_j} + \frac{\partial \overline{u_j}}{\partial x_i}\right) - \rho \overline{u_i' u_j'}\right] + F_i, \tag{1}$$

where ρ is the density; t is the time; $\overline{u_i}$ and $\overline{u_j}$ are the mean velocity components; $\overline{p}$ is the mean pressure; x_i and x_j are the coordinate directions; μ is the dynamic viscosity; F_i is the body force component; $-\rho \overline{u_i' u_j'}$ is the Reynolds stress; and u_j' and u_j' are the fluctuating velocity components.

The RNG $k-\varepsilon$ turbulent model is chosen to solve the flow in the pump because this model is suitable for solving complicated flows such as rotating flows, separated flows, and vortex flows [42–46]. The k equation and ε equation of the RNG $k-\varepsilon$ turbulent model are shown as follows:

$$\rho \frac{\partial k}{\partial t} + \rho \frac{\partial k \overline{u_i}}{\partial x_i} = \frac{\partial}{\partial x_j}\left[\left(\mu + \frac{\mu_t}{\sigma_k}\right)\frac{\partial k}{\partial x_j}\right] + G_k - \rho\varepsilon,$$

$$\rho \frac{\partial \varepsilon}{\partial t} + \rho \frac{\partial \varepsilon \overline{u_i}}{\partial x_i} = \frac{\partial}{\partial x_j}\left[\left(\mu + \frac{\mu_t}{\sigma_\varepsilon}\right)\frac{\partial \varepsilon}{\partial x_j}\right] + \frac{C_{1\varepsilon}\varepsilon}{k} G_k - C_{2\varepsilon}\rho \frac{\varepsilon^2}{k}, \tag{2}$$

where G_k is the turbulent kinetic energy production term; $C_{1\varepsilon}$ is an empirical constant; $C_{2\varepsilon}$ is an empirical constant; σ_k is the corresponding Prandtl number for turbulent kinetic energy k; and σ_ε is the corresponding Prandtl number for the turbulent kinetic energy dissipation rate ε.

2.2. Computational Domain and Boundary Conditions. The computational domain of the flow field in an axial flow pump is composed of a straight inlet pipe, conical inlet pipe, impeller and impeller chamber, guide vane, bent outlet pipe, and straight outlet pipe (Figure 1). The inlet boundary for the flow field calculation of an axial flow pump is set at the inlet section of the straight inlet pipe. The discharge rate is known, and the flow velocity distribution is uniform at the inlet section; thus, the velocity inlet boundary condition is adopted [47]. The outlet boundary for the flow field calculation of the axial flow pump is set at the outlet section of the straight outlet pipe, where the flow is fully developed; thus, the outflow boundary condition is adopted. In the flow field calculation, the sidewalls of the pipes, impeller chamber, guide vane, pump shaft, fair water caps at the impeller inlet, and the guide vane outlet are solid and are treated according to the conditions for a solid wall [48]. Since the axial flow pump impeller rotates periodically, the rotating walls such as the impeller blade and hub adopt the moving wall boundary condition, and the rotation speed and direction are the same as those of the impeller.

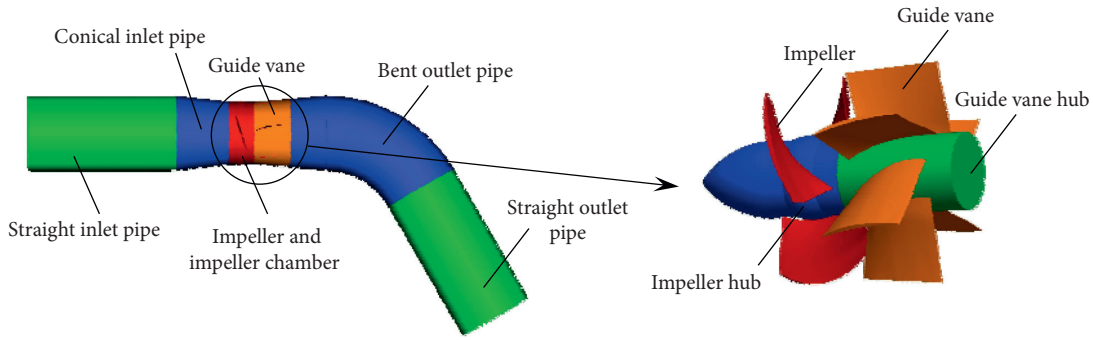

Figure 1: Computational domain for an axial flow pump.

2.3. Numerical Setting and Calculation Accuracy. The GAMBIT software is used to generate the mesh for the computational domain. The shapes of the straight inlet pipe, conical inlet pipe, bent outlet pipe, and straight outlet pipe are simple; structured hexahedral meshes are applied. The shapes of the impeller and guide vane are complicated; unstructured meshes are applied. Moreover, since the flows in the impeller and guide vane are very complicated, the meshes are subject to local refinement. The $y+$ value of the near-wall mesh scale is in the range of 20–70, which meets the requirement of numerical simulation. During the numerical simulation, a first-order upwind difference scheme is used to solve the convection-diffusion equation, the SIMPLEC algorithm is used to solve the pressure-velocity coupling equations, and the convergence precision is set to 1×10^{-7}.

A mesh independence verification was performed to ensure the calculation accuracy and computation efficiency. The calculation parameters for the TJ04-ZL-06 pump model are as follows: the diameter and rated speed of the pump impeller are 0.3 m and 1450 r/min, respectively, and the design discharge rate Q is 0.375 m^3/s for a blade angle of -2° according to model test results obtained for the test bed of Beifang Investigation, Design and Research Co., Ltd., Tianjing, China [39].

Pump segment efficiency is an important energy performance index of pump, which is used as the judgment basis for mesh independence analysis. The calculation formula of pump segment efficiency is as follows:

$$\eta_{bd} = \frac{\rho g Q H_{bd}}{P_{bz}} \times 100\%, \tag{3}$$

where η_{bd} is the pump segment efficiency; g is the gravitational acceleration; Q is the discharge rate; H_{bd} is the pump segment head; and P_{bz} is the pump shaft power.

Table 1 shows the relationship between the pump segment efficiency and grid number under the abovementioned conditions. When the grid number of computational domain exceeds 1,863,552, the pump segment efficiency changes only slightly. Based on the verification results, the grid number of the entire calculation domain is set to approximately 1,860,000 in the calculations; the grid numbers of each component are shown in Table 2. The grid generation of the computational domain is shown in Figure 2.

Based on the abovementioned numerical method and setting, the pump efficiency of pump model TJ04-ZL-06 was calculated for a discharge rate between $0.8\eta_{bd}$ and $1.2\eta_{bd}$. Based on the calculated results, the relationship between the discharge rate and pump segment efficiency is shown in Figure 3; the flow fields in the pump are shown in Figure 4. It could be seen that the pump segment efficiency increases firstly and then decreases as the discharge rate increases. Because the inlet angle of guide vane does not match with the flow direction from the impeller outlet under the off-design conditions, there will be vortex on the back of guide vane under the condition of small discharge rate, and there will be vortex on the front of guide vane under the condition of large discharge rate. The comparison of numerical calculation and model test results is shown in Figure 3. The test data of TJ04-ZL-06 pump model is from the model pump test on the same test bed for the south-to-north water diversion [39]. Clearly, the trends observed for the numerical simulation are consistent with those for the model test, and the two curves are similar, indicating that the numerical results are reliable.

3. Research Scheme

To satisfy hydraulic design requirements and structure demands, the guide vane is divided into an inlet segment, middle segment, and outlet segment (Figure 5). The inlet segment is used to adjust the inlet angle of the guide vane in order to match the flow direction of the impeller outlet under off-design conditions. The middle segment is used to fix the bearing support. The outlet segment, which is used to adjust the circulation of the guide vane outlet, is fixed in this paper.

In Figure 5, the axial chord of the guide vane is H, and the inlet segment axial chord of the guide vane is h (Figure 4). For a given H, a larger h corresponds to a shorter fixed region (middle and outlet segments), and the support function of the guide vane will be negatively affected. However, a smaller h corresponds to a weaker adjustment effect for the inlet angle of the guide vane. Therefore, h values of $0.1H$, $0.2H$, $0.25H$, and $0.33H$ were employed to study the influence of h on the hydraulic performance of the axial flow pump.

The inlet angle of the guide vane β_0 for the model pump TJ04-ZL-06 is determined based on the design conditions

Table 1: Relationship between outlet conduit hydraulic loss and grid number.

Grid number	788,332	967,806	1,262,519	1,516,022	1,863,552	1,966,585	2,256,251
Pump segment efficiency (%)	85.73	85.67	85.24	84.51	84.16	84.12	84.12

Table 2: Detailed mesh information of computational domain.

Domain	Straight inlet pipe	Conical inlet pipe	Impeller and impeller chamber	Guide vane	Bent outlet pipe	Straight outlet pipe
Grid number ($\times 10^3$)	203	252	317	392	495	201

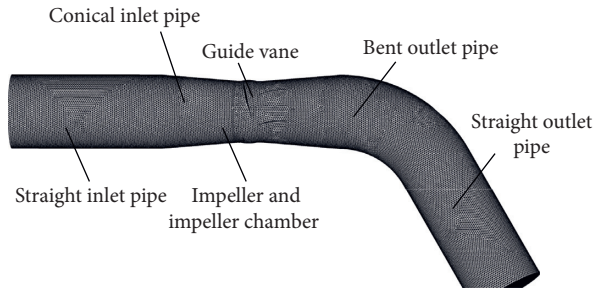

Figure 2: Grid generation of the computational domain.

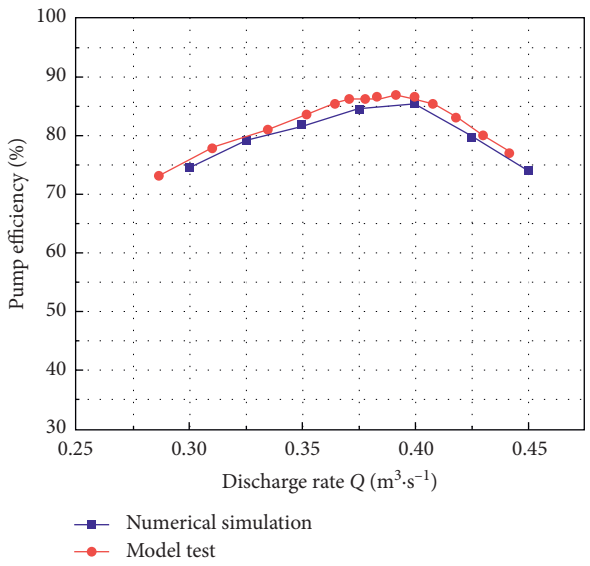

Figure 3: Comparison of the numerical simulation and model test results.

(Figure 6). In this paper, the inlet angle of the guide vane β_0 is defined as 0°. Based on β_0, if the inlet segment of the guide vane is rotated counterclockwise (Figure 6(b)), the inlet angle adjustment $\Delta\beta$ is positive; if the inlet segment of the guide vane is rotated clockwise (Figure 6(c)), the angle adjustment $\Delta\beta$ is negative. According to the velocity triangle at the impeller outlet, when the pump operates under a flow that is larger than the design condition, β_0 does not match the absolute velocity of the flow at the impeller outlet, and the inlet segment needs to rotate clockwise. By contrast, when the pump operates under smaller flow conditions, the inlet segment needs to rotate counterclockwise. In an actual system, the pump at a low head pumping station usually operates under a large flow; thus, the pump system efficiency is low [49, 50]. To improve the efficiency, the study in this paper places an additional emphasis on the influence of $\Delta\beta$ on the pump segment efficiency under large flow conditions; therefore, $\Delta\beta$ is taken as −15°, −10°, −5°, 0°, and +5°.

The inlet segment of the guide vane is based on two geometrical parameters: the inlet segment axial chord h and the inlet angle adjustment $\Delta\beta$. The calculation schemes are determined by h and $\Delta\beta$, the h is selected as 0.1H, 0.2H, 0.25H, and 0.33H, and the $\Delta\beta$ is selected as +5°, 0°, −5°, −10°, and −15°. The combination of the two factors forms a total of 20 calculation schemes. Based on the model pump TJ04-ZL-06 for a blade angle of −2°, the calculation discharge rates for the schemes are taken as 0.30 m^3/s, 0.325 m^3/s, 0.35 m^3/s, 0.375 m^3/s, 0.40 m^3/s, 0.425 m^3/s, and 0.45 m^3/s. Note that when $\Delta\beta = 0°$, the scheme is the same as the original guide vane.

4. Results and Analysis

4.1. Calculation Results. The pump segment energy performance for each calculation scheme was calculated using a 3D turbulent flow numerical simulation. The curves of pump segment efficiency η_{bd} and discharge rate Q for different inlet segment axial chords h and inlet angle adjustments $\Delta\beta$ are shown in Figure 7.

4.2. Influence of Inlet Segment Axial Chord on Pump Segment Efficiency. Based on the calculation results, the pump segment efficiency η_{bd} and inlet segment axial chord h for different values of discharge rate Q are shown in Figure 8. It can be seen that h has a strong effect on η_{bd}. When the discharge rate is smaller than the optimum operating discharge rate, if $\Delta\beta > 0°$, η_{bd} will increase slightly as h increases; if $\Delta\beta < 0°$, η_{bd} will gradually decrease as h increases. A smaller $\Delta\beta$ corresponds to a greater decrease in η_{bd}. For a discharge rate that is larger than the optimum operating discharge rate, if $\Delta\beta > 0°$, η_{bd} will decrease as h increases; if $\Delta\beta < 0°$, η_{bd} gradually increases as h increases. In this case, a smaller $\Delta\beta$ corresponds to a greater increase in η_{bd}. Figure 8 shows that regardless of whether η_{bd} increases or decreases with increasing h, when $h > 0.25H$, the influence of h on η_{bd} decreases. Therefore, considering the support function and hydraulic performance of the guide vane, the inlet segment axial chord h is taken as 0.25H.

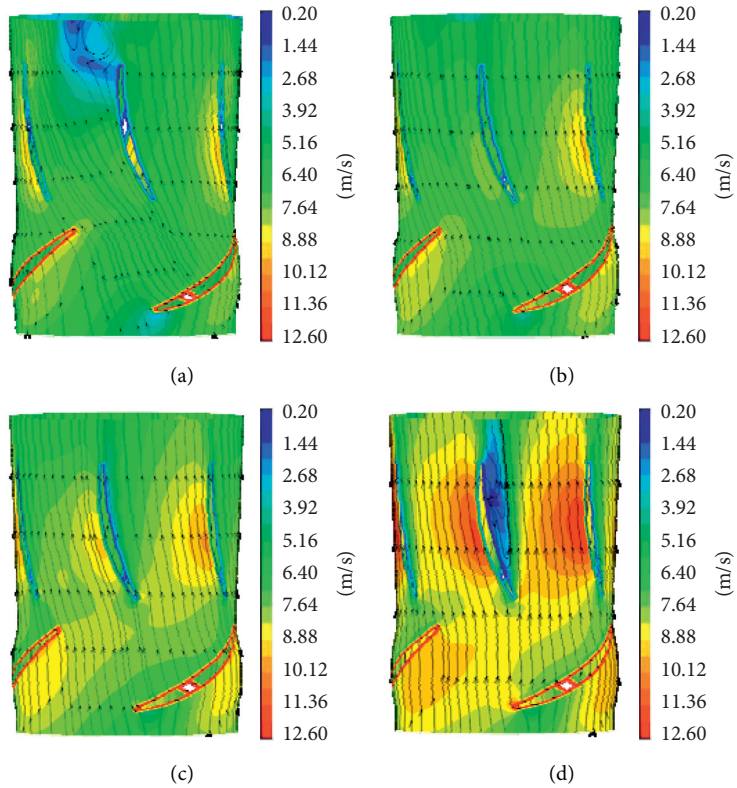

Figure 4: Flow fields in the pump segment under different conditions of discharge rates. (a) $Q = 0.30\ m^3/s$, (b) $Q = 0.35\ m^3/s$, (c) $Q = 0.40\ m^3/s$, and (d) $Q = 0.45\ m^3/s$.

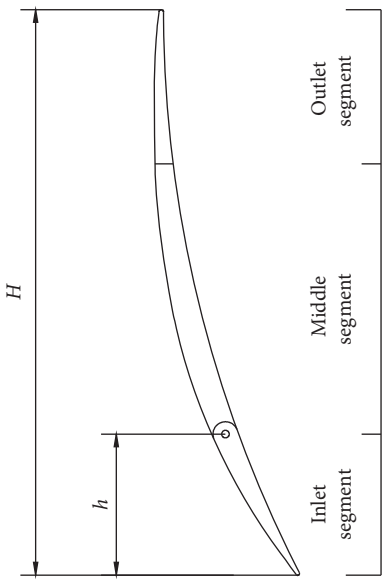

Figure 5: Segmentation of the guide vane.

4.3. Influence of Inlet Angle Adjustment on Pump Segment Efficiency. Based on the calculation results, the pump segment efficiency η_{bd} and inlet angle adjustment $\Delta\beta$ for different discharge rate Q values with $h = 0.25H$ are shown in Figure 9. It could be seen as follows: as the inlet angle adjustment $\Delta\beta$ increases, the pump segment efficiencies η_{bd} increase when the discharge rates Q are $0.30\ m^3/s$, $0.325\ m^3/s$, and $0.35\ m^3/s$, the pump segment efficiencies η_{bd} are basically constant when the discharge rates Q are $0.375\ m^3/s$ and $0.40\ m^3/s$, and the pump segment efficiencies η_{bd} decrease when the discharge rates Q are $0.425\ m^3/s$ and $0.45\ m^3/s$. When the discharge rate is smaller than the optimum operating discharge rate, a larger $\Delta\beta$ corresponds to a greater η_{bd}; when the discharge rate is larger than the optimum operating discharge rate, a smaller $\Delta\beta$ corresponds to a greater η_{bd}.

Under the condition of $h = 0.25H$, the flow fields in the pump at different discharge rates when the inlet angle adjustments $\Delta\beta$ are $+5^\circ$ and -10° are shown in Figures 10 and 11, respectively. Comparing the flow fields in Figures 4, 10, and 11, it could be seen as follows: under the same discharge rate condition, the flow fields in the impeller are the same for different inlet angle adjustments; when the discharge rates are $0.35\ m^3/s$ and $0.40\ m^3/s$, the flow pattern in the guide vane is all good for different inlet angle adjustments, so the pump segment efficiency changes little as the inlet angle adjustment increases (Figure 9); when the discharge rate is 0.30 m3/s, there is flow separation on the back of the guide vane, and there is a big range of vortex when the inlet angle adjustment is -10°; the smaller the inlet angle adjustment, the worse the flow separation and the bigger the energy loss, therefore the pump segment efficiency decreases as the inlet angle adjustment decreases at the small discharge rate (Figure 9); when the discharge rate is 0.45 m3/s, there is flow separation on the front of the guide vane; there is a big range of vortex when the inlet

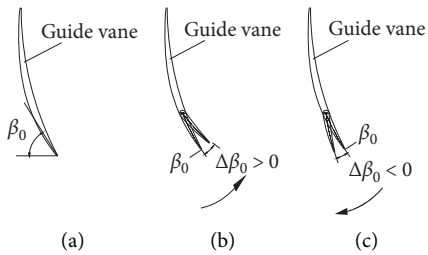

Figure 6: The datum and turn direction for adjusting the guide vane inlet angle. (a) Inlet angle of the guide vane. (b) Counterclockwise rotation. (c) Clockwise rotation.

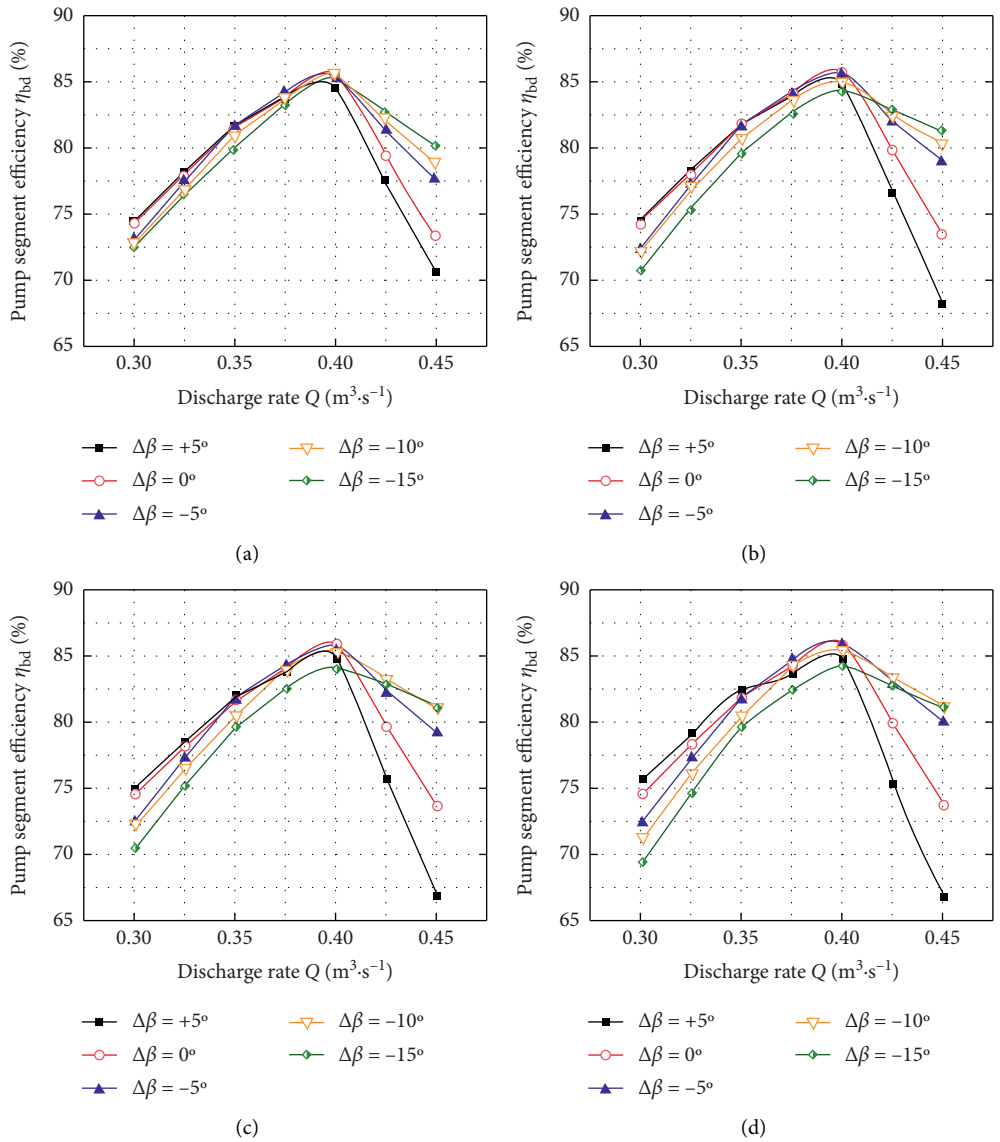

Figure 7: $Q \sim \eta_{bd}$ curves for the different calculation schemes. (a) $h = 0.10H$. (b) $h = 0.20H$. (c) $h = 0.25H$. (d) $h = 0.33H$.

angle adjustment is +5°; the pump segment efficiency decreases dramatically; the bigger the inlet angle adjustment, the worse the flow separation and the bigger the energy loss, so the pump segment efficiency decreases as the inlet angle adjustment increases at the large discharge rate (Figure 9).

4.4. Matching Relation of the Guide Vane Inlet Angle and the Impeller Outlet Flow Direction

4.4.1. Design Working Condition. The relationship between the guide vane inlet angle and the impeller outlet flow direction for an axial flow pump under optimum operating conditions is

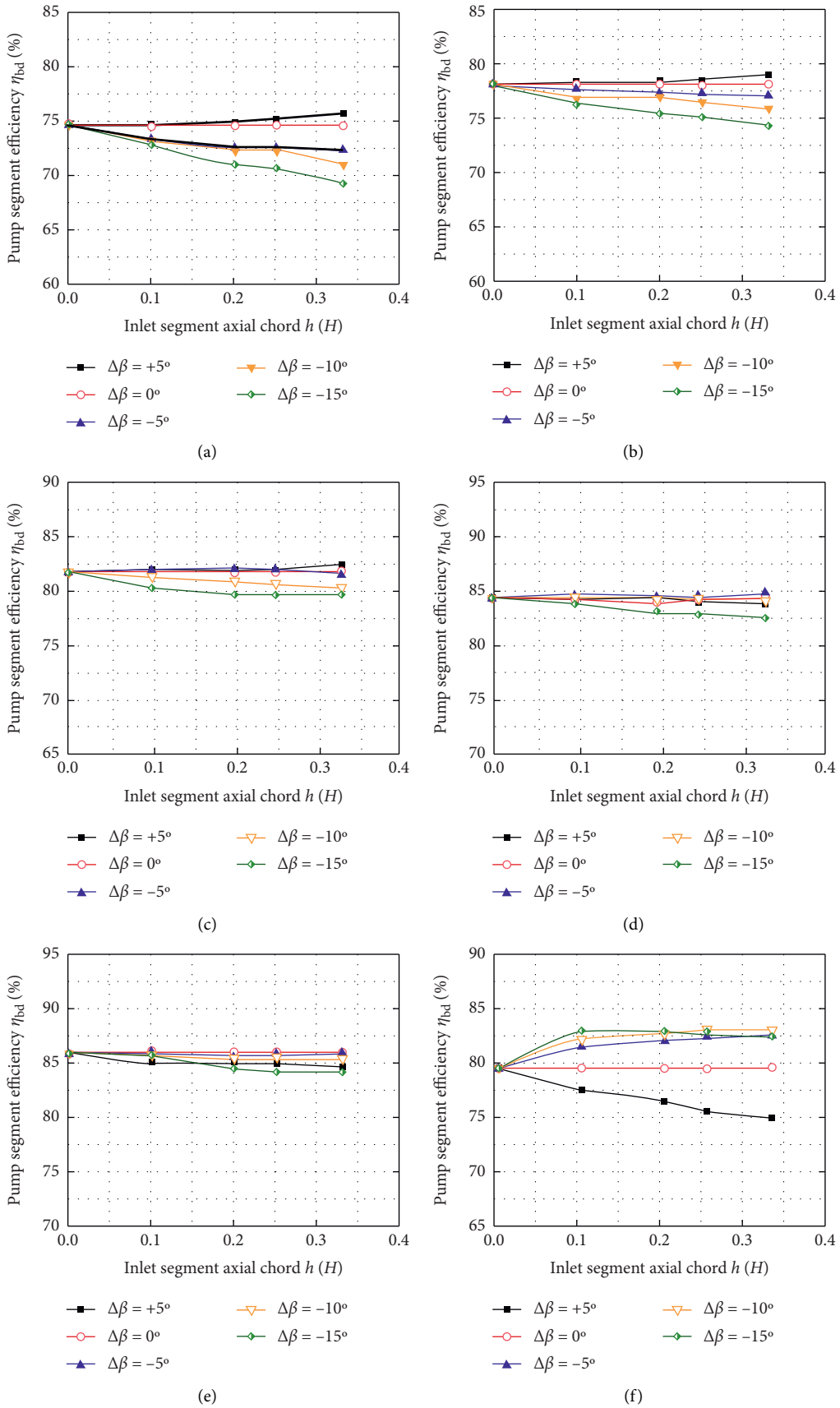

Figure 8: Continued.

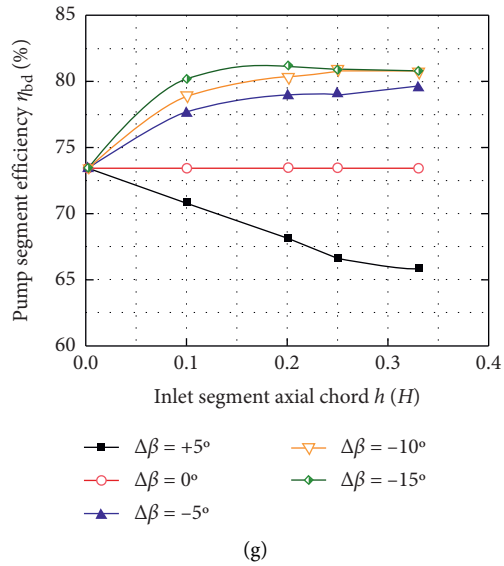

(g)

FIGURE 8: $\eta_{bd} \sim h$ curves for each calculation scheme. (a) $Q = 0.30\ m^3/s$, (b) $Q = 0.325\ m^3/s$, (c) $Q = 0.35\ m^3/s$, (d) $Q = 0.375\ m^3/s$, (e) $Q = 0.40\ m^3/s$, (f) $Q = 0.425\ m^3/s$, and (g) $Q = 0.45\ m^3/s$.

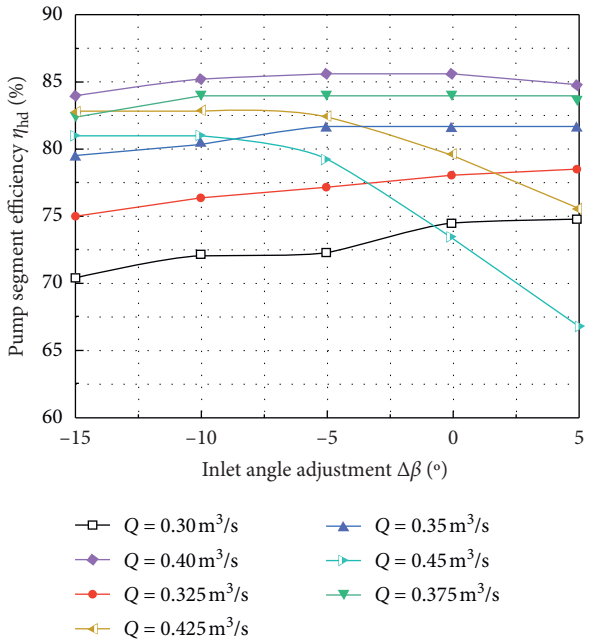

FIGURE 9: $\eta_{bd} \sim \Delta\beta$ curves for different discharge rates when $h = 0.25H$.

shown in Figure 12(a). In the figure, β_0 is the inlet angle of the guide vane under the design working conditions, v_0, w_0, and u are the absolute velocity, relative velocity, and transport velocity, respectively, of the impeller outlet flow under the design working conditions, and α_0 is the angle between v_0 and u. Obviously, when the axial flow pump operates under the design working conditions, β_0 is equal to α_0, i.e., the inlet angle of the guide vane matches the flow direction of the impeller outlet.

4.4.2. Smaller Discharge Condition. The relationship between the guide vane inlet angle and the impeller outlet flow direction for an axial flow pump with a smaller discharge rate is shown in Figure 12(b). When the axial flow pump operates with a smaller discharge rate, the axial velocity at the impeller outlet is v_{ms}, and the absolute velocity of the impeller outlet flow and the angle between the absolute velocity and transport velocity are v_s and α_s, respectively. At this point, because α_s less than $\alpha_0$and β_0 differs fromα_s, the flow strikes the pressure side of the guide vane. Flow separation and vortices will simultaneously occur on the vacuum side of the guide vane, resulting in an additional hydraulic loss for the guide vane. To ensure that the inlet angle of the guide vane matches the flow direction of the impeller outlet for a smaller discharge rate, the inlet angle must be changed by a certain angle counterclockwise based on β_0, as shown by the dotted line in Figure 12(b).

4.4.3. Larger Discharge Rate Condition. The relationship between the guide vane inlet angle and the impeller outlet flow direction for an axial flow pump with a larger discharge rate is shown in Figure 12(c). When the axial flow pump operates with a larger discharge rate, the axial velocity at the impeller outlet is v_{mL}, and the absolute velocity of the impeller outlet flow and the angle between the absolute velocity and transport velocity are v_L and α_L, respectively. At this point, because α_L larger than α_0 and β_0 differs from α_L, the flow strikes the vacuum side of the guide vane. Flow separation and vortices will simultaneously arise on the pressure side of the guide vane, resulting in additional hydraulic loss for the guide vane. To match the guide vane inlet angle with the impeller outlet flow direction for a large discharge rate, the inlet angle must change by a certain angle clockwise based on β_0, as shown by the dotted line in Figure 12(c).

4.5. Influence of the Inlet Angle on the Guide Vane Flow Field. For $Q = 0.45\ m^3/s$, a 3D steady turbulent flow numerical simulation was performed for the axial flow pump with

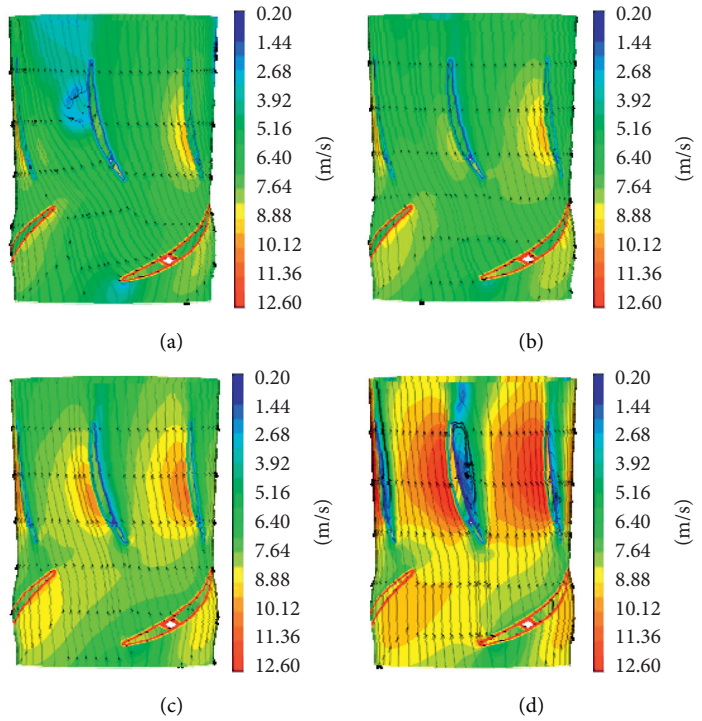

Figure 10: Flow fields in the pump segment under different conditions of discharge rates ($\Delta\beta = +5^{\circ}$, $h = 0.25H$). (a) $Q = 0.30\ m^3/s$, (b) $Q = 0.35\ m^3/s$, (c) $Q = 0.40\ m^3/s$, and (d) $Q = 0.45\ m^3/s$.

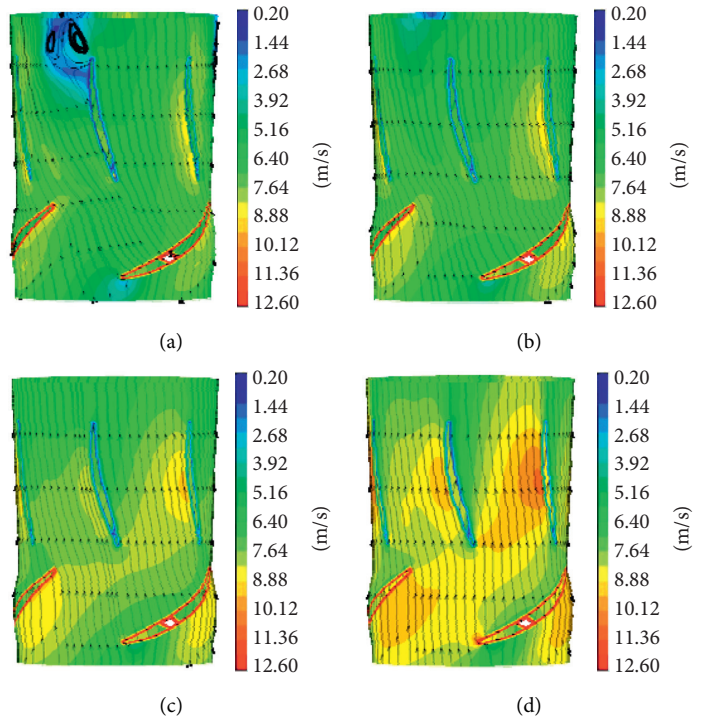

Figure 11: Flow fields in the pump segment under different conditions of discharge rates ($\Delta\beta = -10^{\circ}$, $h = 0.25H$). (a) $Q = 0.30\ m^3/s$, (b) $Q = 0.35\ m^3/s$, (c) $Q = 0.40\ m^3/s$, and (d) $Q = 0.45\ m^3/s$.

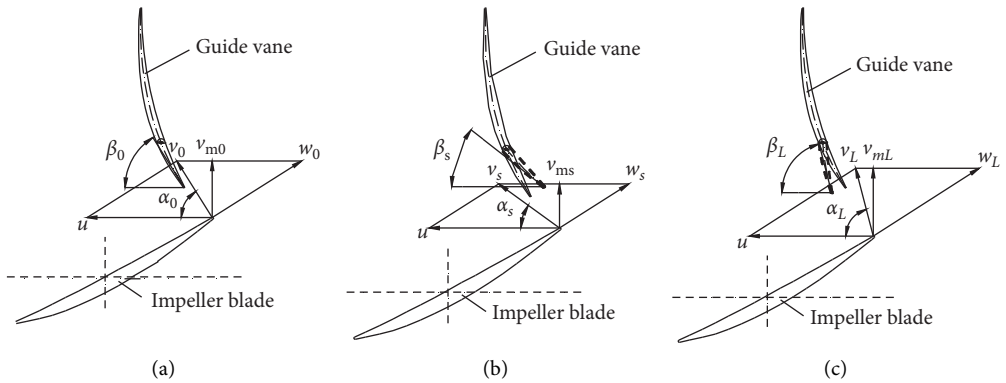

Figure 12: Matching relationships between the guide vane inlet angle and the impeller outlet flow direction. (a) Design discharge rate condition. (b) Smaller discharge rate condition ($\alpha_s < \alpha_0$). (c) Larger discharge rate condition ($\alpha_L > \alpha_0$).

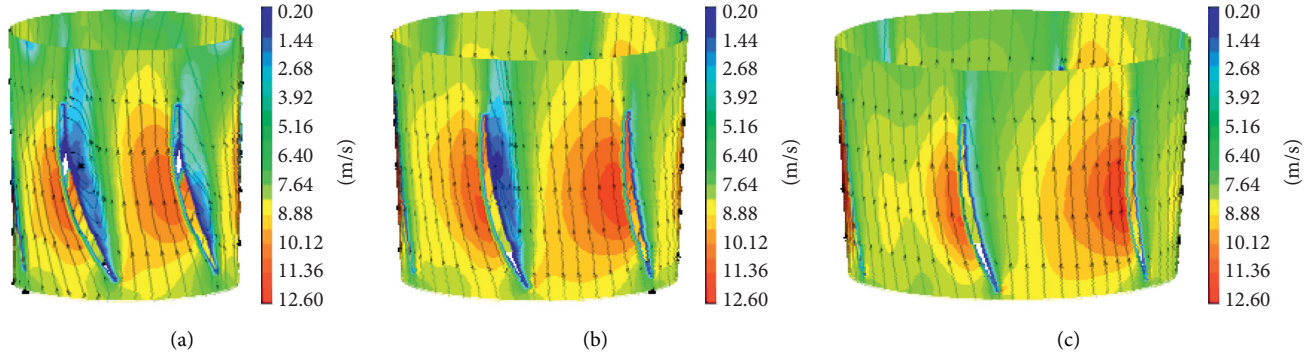

Figure 13: Flow fields of the three tori of the guide vane ($\Delta\beta = 0^\circ$). (a) Inner torus. (b) Middle torus. (c) Outer torus.

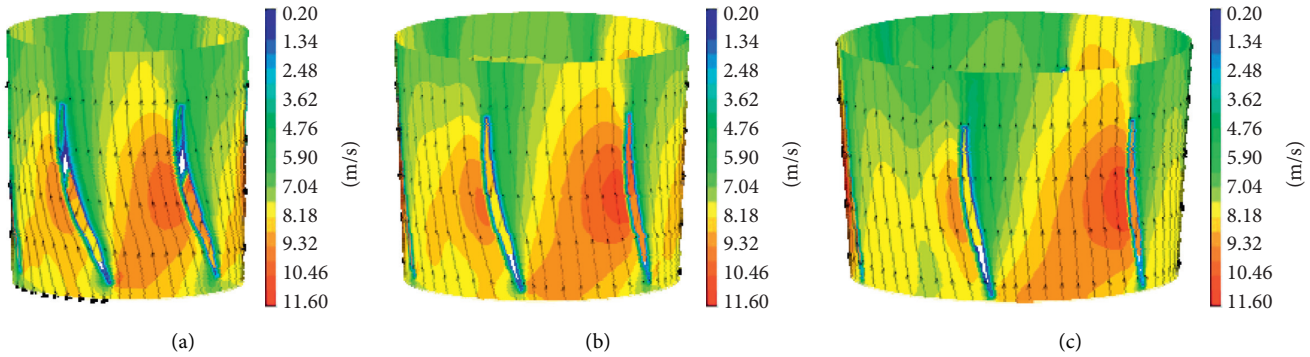

Figure 14: Flow fields of the three tori of the guide vane ($\Delta\beta = -10^\circ$). (a) Inner torus. (b) Middle torus. (c) Outer torus.

$\Delta\beta = 0^\circ$ and $\Delta\beta = -10^\circ$. For ease of analysis, three tori are chosen between the hub and the rim of the guide vane as follows: inner torus (near the hub), middle torus (between the hub and rim), and outer torus (near the rim).

The flow fields of the three tori of the guide vane for $\Delta\beta = 0^\circ$ and $\Delta\beta = -10^\circ$ are shown in Figures 13 and 14, respectively. The figures show that for the larger discharge rate condition, when $\Delta\beta = 0^\circ$, the inlet angle of the guide vane does not match the flow direction of the impeller outlet; thus, the vacuum side of the guide vane is struck by the flow. Flow separation and vortices occur simultaneously on the pressure side of the guide vane; therefore, the hydraulic loss of the guide vane is increased. For $\Delta\beta = -10^\circ$, the inlet angle of the guide vane matches the flow direction of the impeller outlet, and the flow to the adjacent guide vane is smooth. Essentially, no collisions or vortices occur, the flow pattern in the guide vane is substantially improved, and the hydraulic loss of the guide vane is reduced.

At the same time, the unsteady flow numerical simulation was performed for the axial flow pump with $\Delta\beta = 0^\circ$ and $\Delta\beta = -10^\circ$ when the discharge rate Q is 0.45 m^3/s. The total calculation time was set to 8 times the rotation period of the impeller, the total time T is 0.33103448 s, and the time step t was set as $3.448275833 \times 10^{-4}$ which is the time required for

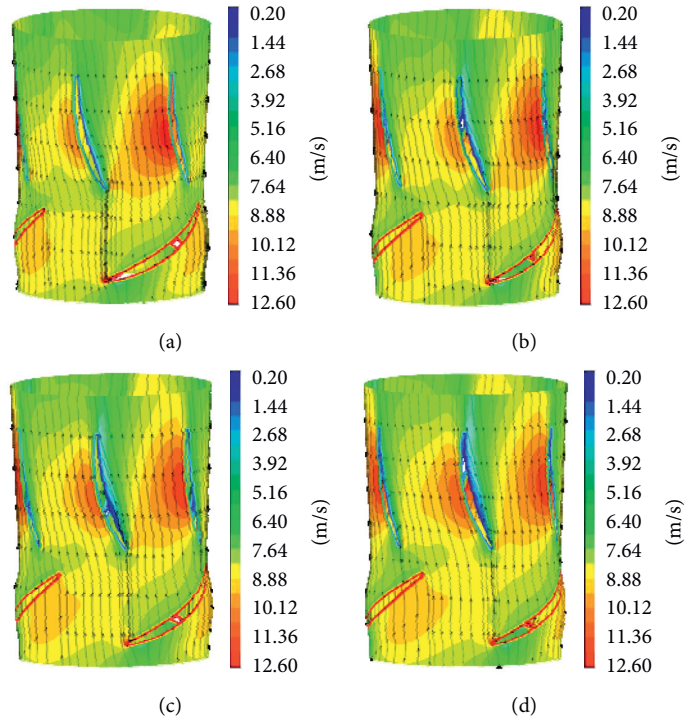

FIGURE 15: Flow fields of middle tori of the pump segment at different time in one period T ($\Delta\beta = 0^\circ$). (a) $t = 1/4\ T$, (b) $t = 2/4\ T$, (c) $t = 3/4\ T$, and (d) $t = T$.

the impeller to rotate 3°. In consideration of the stability of the flow field calculation, the internal flow field was analyzed after 4 rotation periods. The flow fields of middle tori of pump segment at different time in one period T are respectively shown in Figures 15 and 16 for $\Delta\beta = 0^\circ$ and $\Delta\beta = -10^\circ$ by unsteady flow numerical simulation. When the inlet angle adjustment $\Delta\beta$ is 0°, there is a tendency of vortexes on the front of the guide vane at 1/4 T, and the vortex is appeared on the front of the guide vane at 3/4 T; it is basically consistent with the results of steady flow numerical simulation. When the inlet angle adjustment $\Delta\beta$ is −10°, there is no vortex on the front of the guide vane during the full period; it is the same with the results of steady flow numerical simulation.

4.6. Influence of the Guide Vane Inlet Angle on Hydraulic Loss and Efficiency

4.6.1. Influence of $\Delta\beta$ on the Hydraulic Loss of the Guide Vane Δh_{dy}. In the range of considered working conditions, when $Q = 0.45\ \mathrm{m}^3/\mathrm{s}$, the inlet angle adjustment $\Delta\beta$ has a strong effect on pump segment efficiency η_{bd}. Therefore, this working condition is chosen for analysis. The curves of $\eta_{bd} \sim \Delta\beta$ and $\Delta h_{dy} \sim \Delta\beta$ for different h values under the chosen working condition are shown in Figure 17. Over the range of −15° to +5° for $\Delta\beta$, the hydraulic loss of the guide vane Δh_{dy} increases substantially as $\Delta\beta$ increases, while η_{bd} decreases dramatically. Δh_{dy} increases under the larger discharge rate condition because as $\Delta\beta$ increases, the mismatch between the inlet angle of the guide vane and the flow direction of the impeller outlet increases, the flow impact and vortex in the guide vane become greater (Figure 13), and thus, Δh_{dy} increases.

4.6.2. Influence of Δh_{dy} on the Guide Vane Efficiency η_{dy} and η_{bd}. For $h = 0.25H$, curves of $\eta_{yl} \sim Q$, $\eta_{bd} \sim Q$, and $\Delta h_{dy} \sim Q$ for each calculation scheme are shown in Figure 18. The main energy performance parameters for $\Delta\beta = 0^\circ$ and $\Delta\beta = -10^\circ$ for the pump segment with $Q = 0.45\ \mathrm{m}^3/\mathrm{s}$ are listed in Table 3. The impeller heads H_{yl} for $\Delta\beta = 0^\circ$ and $\Delta\beta = -10^\circ$ are approximately equal at 2.66 m and 2.69 m, respectively; when $\Delta\beta$ is adjusted from 0° to −10°, Δh_{dy} decreases from 0.38 m to 0.17 m because the flow pattern in the guide vane is improved.

According to the calculated impeller head H_{yl} and pump shaft power P_{bz}, the impeller efficiency η_{yl} can be calculated as follows:

$$\eta_{yl} = \frac{\rho g Q H_{yl}}{P_{bz}} \times 100\%, \tag{4}$$

where g is the gravitational acceleration; Q is the discharge rate; and P_{bz} is the pump shaft power. The η_{yl} values calculated from formula (4) for $\Delta\beta = 0^\circ$ and $\Delta\beta = -10^\circ$ are listed in Table 3.

Using the calculated Δh_{dy} and η_{yl}, the guide vane efficiency η_{dy} can be determined as follows:

$$\eta_{dy} = \frac{H_{bd}}{H_{yl}} = \frac{H_{yl} - \Delta h_{dy}}{H_{yl}} \times 100\%. \tag{5}$$

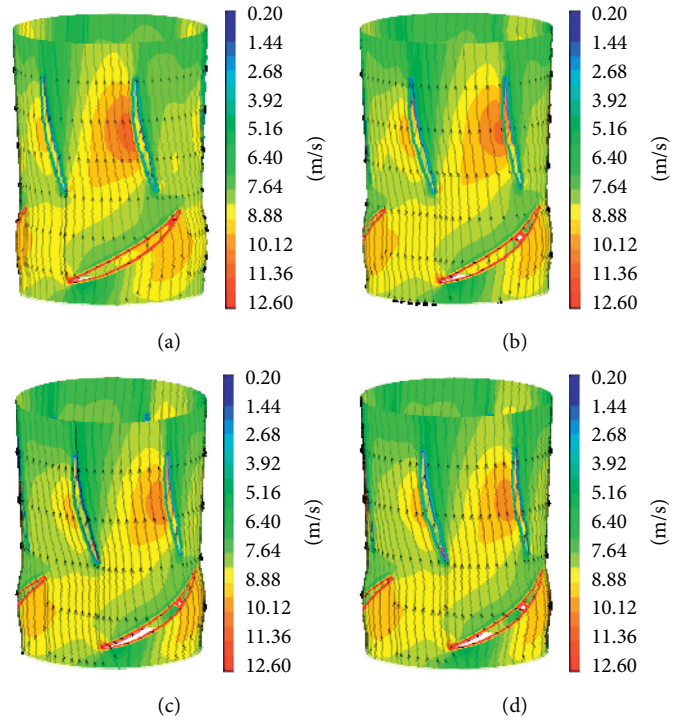

Figure 16: Flow fields of middle tori of the pump segment at different time in one period T ($\Delta\beta = -10^{\circ}$). (a) $t = 1/4\ T$, (b) $t = 2/4\ T$, (c) $t = 3/4\ T$, and (d) $t = T$.

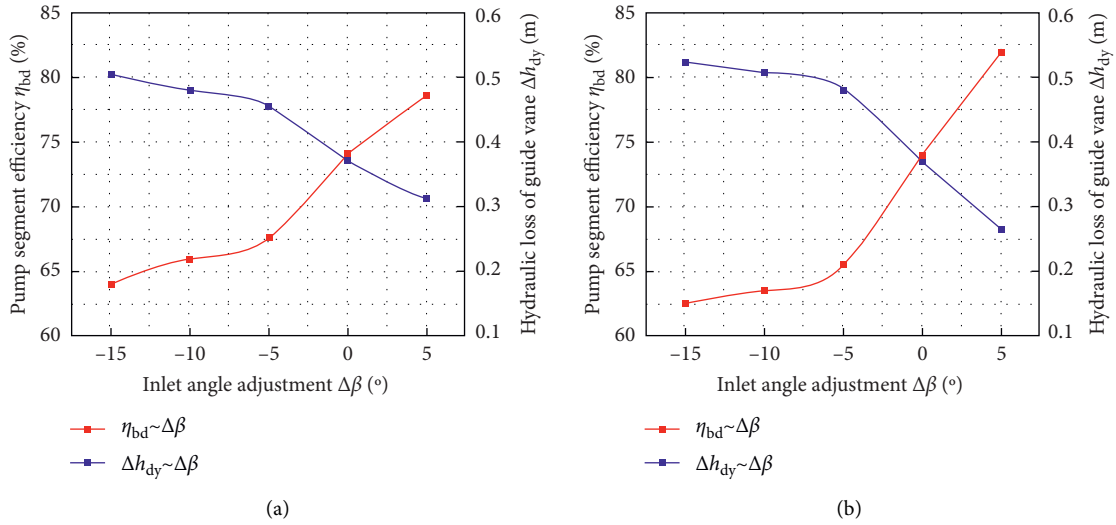

Figure 17: Continued.

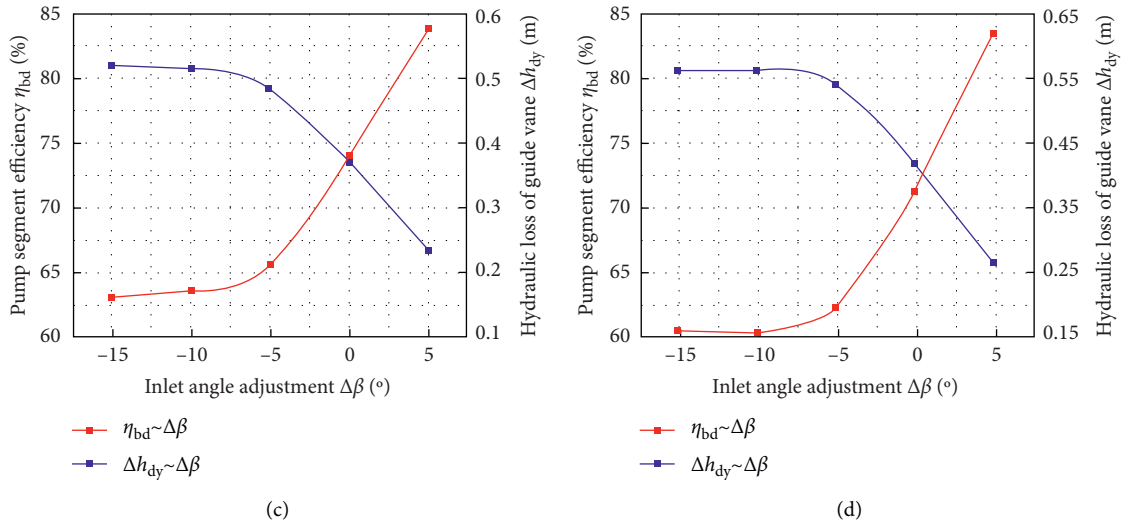

FIGURE 17: $\eta_{bd} \sim \Delta\beta$ and $\Delta h_{dy} \sim \Delta\beta$ curves for different h values. (a) $h = 0.10H$, (b) $h = 0.20H$. (c) $h = 0.25H$, and (d) $h = 0.33H$.

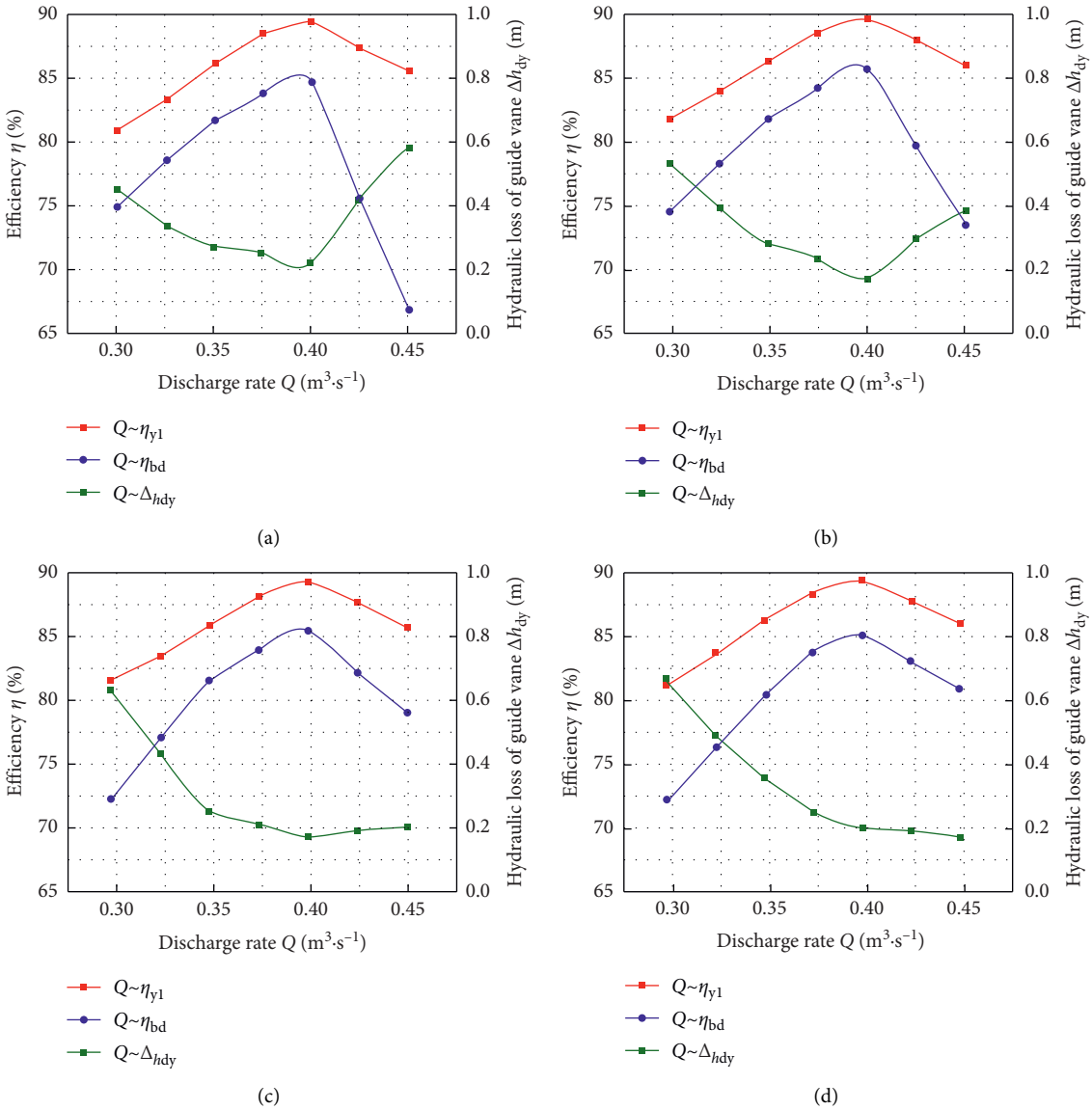

FIGURE 18: Continued.

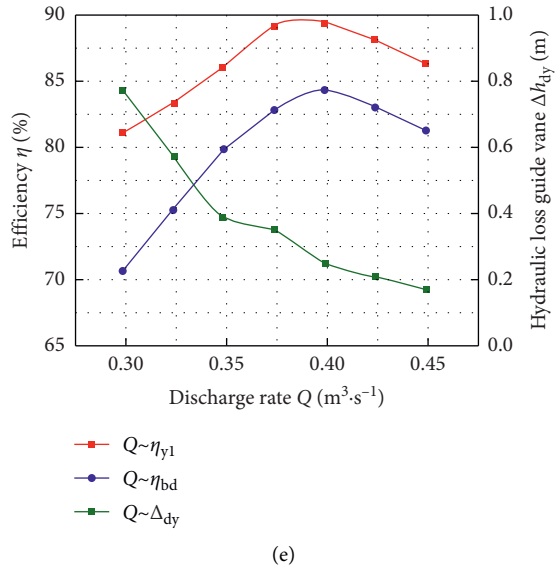

(e)

FIGURE 18: Influence of Δh_{dy} on η_{dy} and η_{bd} for different values of $\Delta\beta$. (a) $\eta_{yl} = +5^{\circ}$, (b) $\eta_{dy} = 0^{\circ}$, (c) $\Delta\beta = -5^{\circ}$, (d) $\eta_{dy} = H_{bd}/H_{yl} = H_{yl} - \Delta h_{dy}/H_{yl} \times 100\% = -10^{\circ}$, and (e) $\Delta\beta = -15^{\circ}$.

TABLE 3: Comparison of energy performance for the pump with $\Delta\beta = 0^{\circ}$ and $\Delta\beta = -10^{\circ}$.

Inlet angle adjustment, $\Delta\beta$ (°)	Impeller head, H_{yl} (m)	Shaft power, P_{bz} (kW)	Hydraulic loss of guide vane, Δh_{dy} (m)	Impeller efficiency, η_{yl} (%)	Pump segment head, H_{bd} (m)	Guide vane efficiency, η_{dy} (%)	Pump segment efficiency, η_{bd} (%)
0°	2.66	13.67	0.38	85.8	2.28	85.7	73.5
−10°	2.69	13.76	0.17	86.2	2.52	93.7	80.9

According to formulas (4) and (5), formula (3) could be transformed as follows:

$$\eta_{bd} = \frac{\rho g Q H_{bd}}{P_{bz}} = \frac{\rho g Q H_{yl}}{P_{bz}} \times \frac{H_{bd}}{H_{yl}} = \eta_{yl} \times \eta_{dy}. \quad (6)$$

Pump segment efficiency η_{bd} is the product of impeller efficiency η_{yl} and guide vane efficiency η_{dy}.

The η_{dy} and η_{bd} values for $\Delta\beta = 0^{\circ}$ and $\Delta\beta = -10^{\circ}$, calculated from formulas (5) and (6), are listed in Table 3.

The abovementioned results indicate that when $\Delta\beta$ is adjusted from 0° to −10°, H_{yl} and η_{yl} are basically unchanged, and the hydraulic performance of impeller is not affected by the inlet segment adjustment of the guide vane. However, when the inlet segment angle is −10°, the inlet angle of guide vane is matched with flow direction at the impeller outlet well, the flow pattern in the guide vane becomes better, and the vortex is eliminated, so the Δh_{dy} decreases from 0.38 m to 0.17 m, and then guide vane efficiency η_{dy} increases from 85.7% to 93.4% and pump segment efficiency η_{bd} improves from 73.5% to 80.9% correspondingly.

5. Conclusions

(1) The inlet segment axial chord h of the guide vane influences the pump segment efficiency η_{bd}. As h increases, η_{bd} increases under smaller discharge rate conditions and decreases under larger discharge rate conditions for $\Delta\beta > 0^{\circ}$; in contrast, η_{bd} decreases under smaller discharge rate conditions and increases under larger discharge rate conditions when $\Delta\beta < 0^{\circ}$. When $h > 0.25H$, the influence of h on η_{bd} weakens.

(2) The inlet angle adjustment $\Delta\beta$ of the guide vane has a strong effect on the pump segment efficiency η_{bd}. When the inlet angle of the guide vane is rotated counterclockwise with respect to the design condition, η_{bd} increases under the smaller discharge rate condition; when the inlet angle of the guide vane is rotated clockwise with respect to the design condition, η_{bd} increases under the larger discharge rate condition. The greater the deviation from the design condition, the larger the influence of $\Delta\beta$ on η_{bd}.

(3) The match between the guide vane inlet angle and the impeller outlet flow direction has a strong influence on the pump segment efficiency η_{bd} because the flow pattern is highly sensitive to deviations in the inlet angle of the guide vane; this change in the flow pattern will directly influence the hydraulic loss of the guide vane.

Data Availability

The data used to support the findings of this study are included within the article.

Conflicts of Interest

The authors declare that they have no conflicts of interest regarding the publication of this paper.

Acknowledgments

This work was supported by the National Natural Science Foundation of China (Grant nos. 51309200, 51779215, and 52079120), a China Postdoctoral Science Foundation Funded Project (Grant no. 2013M540469), and the Jiangsu Planned Projects for Postdoctoral Research Funds (Grant no. 1301021A).

References

[1] C. Wang, W. Shi, X. Wang et al., "Optimal design of multistage centrifugal pump based on the combined energy loss model and computational fluid dynamics," *Applied Energy*, vol. 187, pp. 10–26, 2017.

[2] X. He, W. Jiao, C. Wang, and W. Cao, "Influence of surface roughness on the pump performance based on computational fluid dynamics," *IEEE Access*, vol. 7, pp. 105331–105341, 2019.

[3] C. Wang, X. He, D. Zhang, B. Hu, and W. Shi, "Numerical and experimental study of the self-priming process of a multistage self-priming centrifugal pump," *International Journal of Energy Research*, vol. 43, pp. 1–19, 2019.

[4] H. Yan, X. Su, H. Zhang et al., "Design approach and hydrodynamic characteristics of a novel bionic airfoil," *Ocean Engineering*, vol. 216, Article ID 108076, 2020.

[5] C. Wang, X. He, W. Shi, X. Wang, and N. Qiu, "Numerical study on pressure fluctuation of a multistage centrifugal pump based on whole flow field," *AIP Advances*, vol. 9, Article ID 035118, 2019.

[6] M. T. Shervani-Tabar, M. M. Ettefagh, S. Lotfan, and H. Safarzadeh, "Cavitation intensity monitoring in an axial flow pump based on vibration signals using multi-class support vector machine," *Proceedings of the Institution of Mechanical Engineers, Part C: Journal of Mechanical Engineering Science*, vol. 232, no. 17, pp. 3013–3026, 2018.

[7] Y. Yang, L. Zhou, W. Shi, Z. He, Y. Han, and Y. Xiao, "Interstage difference of pressure pulsation in a three-stage electrical submersible pump," *Journal of Petroleum Science and Engineering*, vol. 196, Article ID 107653, 2020.

[8] C. Wang, B. Hu, Y. Zhu, X. Wang, C. Luo, and L. Cheng, "Numerical study on the gas-water two-phase flow in the self-priming process of self-priming centrifugal pump," *Processes*, vol. 7, no. 6, p. 330, 2019.

[9] F. P. Tang and G. Q. Wang, "Influence of outlet guide vanes upon performances of waterjet axial-flow pump," *Journal of Ship Mechanics*, vol. 10, pp. 19–26, 2006.

[10] F. P. Tang, J. R. Zhou, and B. P. Yan, "Analysis on the recycle energy of back guide vane of axial-flow pump," *Pump Technology*, vol. 3, pp. 19–22, 1995.

[11] Z. Li, M. G. Yang, and X. K. Wang, "Experimental study of guide vane influence on performance of axial-flow pump," *Drainage and Irrigation Machinery*, vol. 27, pp. 15–18, 2009.

[12] J. Hu, S. Huang, and P. S. Wang, "Research on hydrodynamic characteristics of axial waterjet pump with guide vane," *Journal of Hydroelectric Engineering*, vol. 27, pp. 32–36, 2008.

[13] K. Durmus, "Experimental study on regaining the tangential velocity energy of axial flow pump," *Energy Conversion and Management*, vol. 44, pp. 1817–1829, 2003.

[14] Y. X. Zhou and H. F. Xu, "The influence of diffuser on the function of the axial-flow pump," *Water Conservancy & Electric Power Machinery*, vol. 29, pp. 28-29, 2007.

[15] L. J. Shi, F. P. Tang, H. L. Zhou, L. L. Tu, and R. S. Xie, "Axial-flow pump hydraulic analysis and experiment under different swept-angles of guide vane," *Transactions of the Chinese Society of Agricultural Engineering*, vol. 31, pp. 90–95, 2015.

[16] C. J. Liu, Y. S. Wang, and L. X. Wang, "Research on commutating effect optimization of waterjet axial-flow pump stator based on CFD method," *Journal of Ship Mechanics*, vol. 14, pp. 466–471, 2010.

[17] X. Luo, Y. Zheng, and J. Feng, "Hydraulic performance analysis of axial pump outlet guide vane," *Water Resources and Power*, vol. 32, pp. 188–191, 2014.

[18] J. Feng, Y. Zheng, and X. Luo, "Effects of exit guide vane on performance of axial flow pump system," *Water Resources and Power*, vol. 30, pp. 126–128, 2012.

[19] Z. Qian, Y. Wang, W. Huai, and Y. Lee, "Numerical simulation of water flow in an axial flow pump with adjustable guide vanes," *Journal of Mechanical Science and Technology*, vol. 24, no. 4, pp. 971–976, 2010.

[20] F. Yang, C. Liu, F. P. Tang, R. S. Xie, and F. Chen, "Numerical analysis and prediction of hydraulic performance for axial-flow pumping station with adjustable outlet guide vane," *Transactions of the CSAE*, vol. 46, pp. 40–46, 2015.

[21] F. Yang, *Research on Hydraulic Performance and Multi-Objective Optimization Design of Low-Lift Pump System*, Doctoral thesis, Yangzhou China, 2013.

[22] Z. D. Qian, F. Wang, Z. Y. Wang, and W. Zhou, "Experimental study on hydraulic performance of saddle zone in axial flow pump with adjustable guide vane," *Journal of Drainage and Irrigation Machinery Engineering*, vol. 31, pp. 461–465, 2013.

[23] X. F. Guan, *Axial Flow Pump and Diagonal Flow Pump*, China Aerospace Press, Beijing, China, 2009.

[24] X. He, Y. Zhang, C. Wang et al., "Influence of critical wall roughness on the performance of double-channel sewage pump," *Energies*, vol. 13, no. 2, p. 464, 2020.

[25] H. L. Wang, B. Long, Y. Yang, Y. Xiao, and C. Wang, "Modelling the influence of inlet angle change on the performance of submersible well pumps," *International Journal of Simulation Modelling*, vol. 19, no. 1, pp. 100–111, 2020.

[26] H. Wang, B. Long, C. Wang, C. Han, and L. Li, "Effects of the impeller blade with a slot structure on the centrifugal pump performance," *Energies*, vol. 13, no. 7, p. 1628, 2020.

[27] L. Shi, J. Zhu, F. Tang, and C. Wang, "Multi-disciplinary optimization design of axial-flow pump impellers based on the approximation model," *Energies*, vol. 13, no. 4, p. 779, 2020.

[28] L. Shi, W. Zhang, H. Jiao et al., "Numerical simulation and experimental study on the comparison of the hydraulic characteristics of an axial-flow pump and a full tubular pump," *Renewable Energy*, vol. 153, pp. 1455–1464, 2020.

[29] C. Wang, X. Chen, N. Qiu, Y. Zhu, and W. Shi, "Numerical and experimental study on the pressure fluctuation, vibration, and noise of multistage pump with radial diffuser," *Journal of the Brazilian Society of Mechanical Sciences and Engineering*, vol. 40, p. 481, 2018.

[30] L. Zhou, W. Wang, J. Hang, W. Shi, H. Yan, and Y. Zhu, "Numerical investigation of a high-speed electrical submersible pump with different end clearances," *Water*, vol. 12, p. 1116, 2020.

[31] G. Peng, X. Huang, L. Zhou, G. Zhou, and H. Zhou, "Solid-liquid two-phase flow and wear analysis in a large-scale

centrifugal slurry pump," *Engineering Failure Analysis*, vol. 114, Article ID 104602, 2020.

[32] H. Wang, Z. Qian, D. Zhang, T. Wang, and C. Wang, "Numerical study of the normal impinging water jet at different impinging height, based on Wray-Agarwal turbulence model," *Energies*, vol. 13, no. 7, p. 1744, 2020.

[33] S. Tang, S. Yuan, and Y. Zhu, "Convolutional neural network in intelligent fault diagnosis toward rotatory machinery," *IEEE Access*, vol. 8, no. 1, pp. 86510–86519, 2020.

[34] S. Tang, S. Yuan, and Y. Zhu, "Deep learning-based intelligent fault diagnosis methods toward rotating machinery," *IEEE Access*, vol. 8, no. 1, pp. 9335–9346, 2020.

[35] L. Zhou, K. Deshpande, X. Zhang, and R. K. Agarwal, "Process simulation of chemical looping combustion using ASPEN plus for a mixture of biomass and coal with various oxygen carriers," *Energy*, vol. 195, Article ID 116955, 2020.

[36] L. Zhou, C. Han, L. Bai, W. Shi, and R. Agarwal, "Numerical and experimental study of multiphase transient core-annular flow patterns in a spouted bed," *ASME Journal of Energy Resource Technology*, vol. 142, no. 9, Article ID 092104, 2020.

[37] S. Tang, S. Yuan, and Y. Zhu, "Data preprocessing techniques in convolutional neural network based on fault diagnosis towards rotating machinery," *IEEE Access*, vol. 8, pp. 149487–149496, 2020.

[38] L. Zhou, C. Han, L. Bai, W. Li, M. A. El-Emam, and W. Shi, "CFD-DEM bidirectional coupling simulation and experimental investigation of particle ejections and energy conversion in a spouted bed," *Energy*, vol. 211, Article ID 118672, 2020.

[39] N. Liu, Y. S. Wang, and G. Zhang, *Model Pump Test on the Same Test-Bed for the South-To-North Water Diversion*, China Water Power Press, Beijing, China, 2006.

[40] C.-Y. Ge, J.-J. Wang, X.-P. Gu, and L.-F. Feng, "CFD simulation and PIV measurement of the flow field generated by modified pitched blade turbine impellers," *Chemical Engineering Research and Design*, vol. 92, no. 6, pp. 1027–1036, 2014.

[41] L. Cheng, C. Liu, F. P. Tang, and J. R. Zhou, "3D numerical simulation and performance predication of vertical axial flow pumping station by RNG turbulent model," *Journal of Mechanical Engineering*, vol. 45, no. 3, pp. 252–257, 2009.

[42] Q. G. Chen, Z. Xu, and Y. J. Zhang, "Application of RNG k–ε models in numerical simulation of engineering turbulent flows," *Chinese Quarterly of Mechanics*, vol. 24, pp. 88–95, 2003.

[43] Y. J. Zheng, K. Wang, X. C. Lei, and F. Tang, "3D numerical simulation in inlet passages of pumping station by RNG k–ε turbulent model with wall-function law," *Water Resources and Power*, vol. 26, pp. 123–125, 2008.

[44] Z. H. Xu, Y. L. Wu, N. X. Chen, Y. Liu, L. Liang, and Y. Z. Wu, "Simulation of turbulent flow in pump based on sliding mesh and RNG k–ε model," *Journal of Engineering Thermophyiscs*, vol. 26, pp. 66–68, 2005.

[45] J. Y. Qian, Z. X. Gao, B. Z. Liu, and Z. J. Jin, "Parametric study on fluid dynamics of pilot-control angle globe valve," *ASME Journal of Fluids Engineering*, vol. 140, no. 11, Article ID 111103, 2018.

[46] W. Jiao, L. Cheng, J. Xu, and C. Wang, "Numerical analysis of two-phase flow in the cavitation process of a waterjet propulsion pump system," *Processes*, vol. 7, no. 10, p. 690, 2019.

[47] Z. Z. Han, *Fluent-Example Calculation and Analysis of Fluid Engineering Simulation*, Beijing Institute Technology Press, Beijing, China, 2009.

[48] F. J. Wang, *Computational Fluid Dynamics Analysis: Principle and Application of CFD Software*, Tsinghua University Press, Beijing, China, 2004.

[49] F. P. Tang, C. Liu, L. Chen, and J. R. Zhou, "New selection method of low head pump," *Advanced in Science and Technology of Water Resource*, vol. 21, pp. 41–43, 2001.

[50] X. S. Lv, Z. F. Huang, and W. Shi, "Analysis on error cause of higher pump design head selection for large scale pumping station," *Shanghai Medium and Large Electrical Machines*, vol. 2, pp. 25–28, 2011.